Acta Astronautica 117 (2015) 73–89

Contents lists available at ScienceDirect

Acta Astronautica

journal homepage: www.elsevier.com/locate/actaastro

UWE-3, in-orbit performance and lessons learned of a modular and flexible satellite bus for future pico-satellite formations ☆

S. Busch *, P. Bangert, S. Dombrovski, K. Schilling

Robotics and Telematics, Department of Computer Science, University of Würzburg, Germany

ARTICLE INFO

Article history:
Received 8 January 2015
Received in revised form
19 June 2015
Accepted 3 August 2015
Available online 12 August 2015

Keywords:
Pico-satellite
In-orbit operations
Attitude determination and control
Autonomous groundstation operation

ABSTRACT

Formations of small satellites offer promising perspectives due to improved temporal and spatial coverage and resolution at reasonable costs. The UWE-program addresses in-orbit demonstrations of key technologies to enable formations of cooperating distributed spacecraft at pico-satellite level. In this context, the CubeSat UWE-3 addresses experiments for evaluation of real-time attitude determination and control.

UWE-3 introduces also a modular and flexible pico-satellite bus as a robust and extensible base for future missions. Technical objective was a very low power consumption of the COTS-based system, nevertheless providing a robust performance of this miniature satellite by advanced microprocessor redundancy and fault detection, identification and recovery software. This contribution addresses the UWE-3 design and mission results with emphasis on the operational experiences of the attitude determination and control system.

© 2015 IAA. Published by Elsevier Ltd. All rights reserved.

1. Introduction

Modern miniaturization technologies enable the realization of satellites at continuously decreasing masses. In an extreme case, pico-satellites provide at about 1 kg of mass a fully functional spacecraft. Inherent limitations of performance and increased susceptibility to noise effects are to be compensated by an advanced control and filtering software, as well as by integrating multiple distributed, cooperating pico-satellites [11,12].

The UWE-program (*U*niversity *W*ürzburg's *E*xperimental satellites) develops step-by-step the relevant technologies for such formation flying capabilities at pico-satellite level [13]. The first German pico-satellite UWE-1 (launched 2005) addressed as scientific objective for the optimization of Internet Protocol parameters to the space environment as a basis for the future networked satellites [2]. UWE-2 (launched 2009) focussed on attitude determination techniques, while UWE-3 (launched 2013, Fig. 1) extended this approach to attitude control. Future formations of satellites use a closed loop control in orbit to keep an appropriate topology for efficient measurements with minimum ground control interaction [8].

Abbreviations: ADCS, attitude determination system; COMM, communication system; COTS, commercial of the shelf; ECI, Earth center inertial; EDAC, error detection and recovery; EPS, electrical power system; FDIR, fault-detection, fault-isolation and recovery; GUI, graphical user interface; JTAG/EEM, joint test action group/embedded emulation module; MLI, multilayer insulation; OBC, onboard computer; RMS, root mean square; RSSI, received signal strength indication; SET, single event transient; SEU, single event upset; TNC, terminal node controller; TWU, toggle watchdog unit; UWE, University of Wuerzburg Experimental satellite

☆ This paper was presented during the 65th IAC in Toronto.

* Corresponding author. Tel.: +49 931 31 86719; fax: +49 931 31 86679.
E-mail address: busch@informatik.uni-wuerzburg.de (S. Busch).

http://dx.doi.org/10.1016/j.actaastro.2015.08.002
0094-5765/© 2015 IAA. Published by Elsevier Ltd. All rights reserved.

The niche market of pico-satellites exhibits dramatic growth with about 100 pico- and nano-satellites launched in 2013, and becomes a technology innovation driver in order to enable robust and reliable operations [7].

This contribution addresses at the example of UWE-3 capabilities of the new generation of advanced pico-satellites, offering a flexible and robust design, as well as a performance [4–6] which supports future operational missions. UWE-3 had specific emphasis on the implementation of an efficient attitude determination and control system at minimum mass and power consumption [10]. Its demonstrated in-orbit performance will be described in details, as this will be a crucial component for future pico-satellite formations, promising very good potential to complement as a distributed sensor network the traditional large, multi-functional satellites.

2. UWE-3 architecture and in-orbit performance

Despite its great potential to initiate a paradigm shift in modern space flight, miniaturized satellite technology is still in its infancy. A significant amount of launched CubeSats, especially university built pico-satellites, fail to meet their basic mission objectives in orbit [9]. Limited size, mass, and power budgets are in general critical design drivers regarding processing, communication and attitude control capabilities, and can severely affect reliability due to the increased usage of commercial components with only little provision of redundancies. Typical failure sources reported include insufficient power generation and unrecoverable processor errors. However, Swartwout [9] concludes that, besides raised attention to thermal design aspects and the inherent risks connected to the utilization of commercial-of-the-shelf components, many failures could have been avoided by more elaborate system-level functional testing.

In order to provide a robust base for future pico-satellite missions in the context of the university's UWE-program, the UWE-3 satellite design follows three major design rules: support for testability and maintainability, reasonable level of redundancy, and energy efficiency.

Thus, UWE-3 introduces a generic pico-satellite platform which supports robust and rapid development, integration and testing of the satellite as well as simple maintenance, extension and replacement of subsystems in any configuration during flat-sat development or flight model integration [5]. Fig. 2 displays the building blocks from which according to mission needs related satellite designs can be flexibly

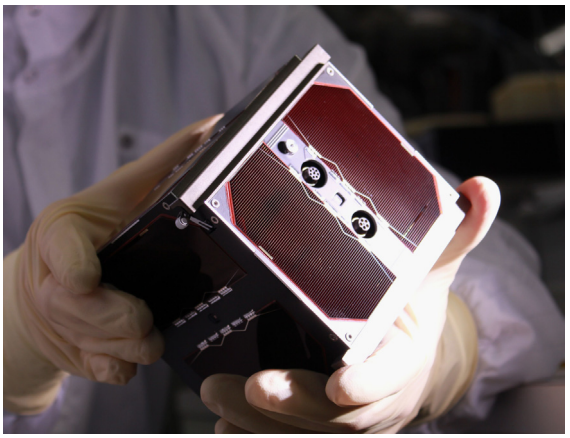


Fig. 1. UWE-3 flight model after integration in Jan. 2013.

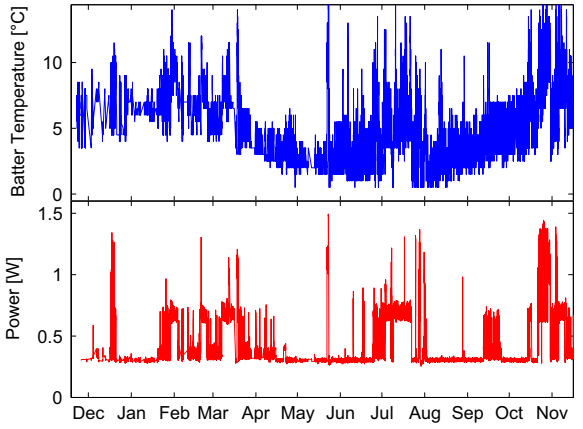


Fig. 3. Seasonal temperature variation in thermally insulated battery case and total power consumption.

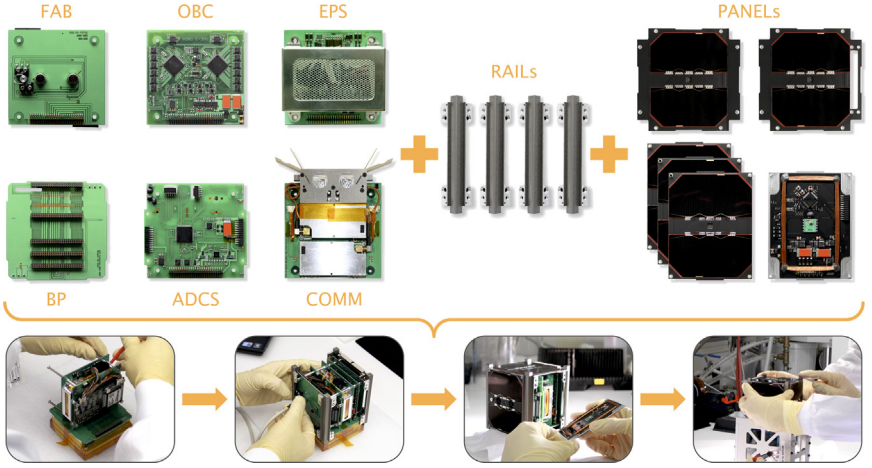


Fig. 2. Overview of the UWE-3 modular architecture.

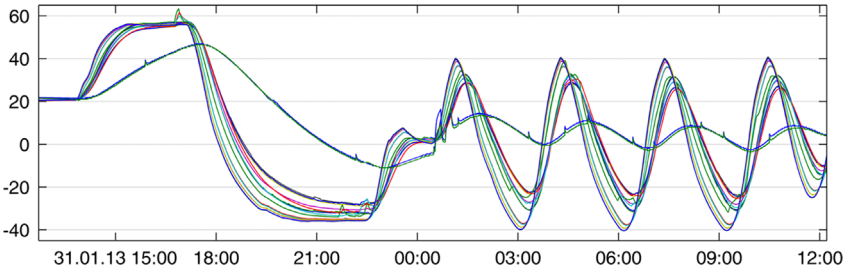


Fig. 4. Thermal vacuum test measurements during proto flight model acceptance showing hot case, cold case and thermal cycling temperature responses. Extreme temperatures are measured on the panels, minor variations are measured in the battery case.

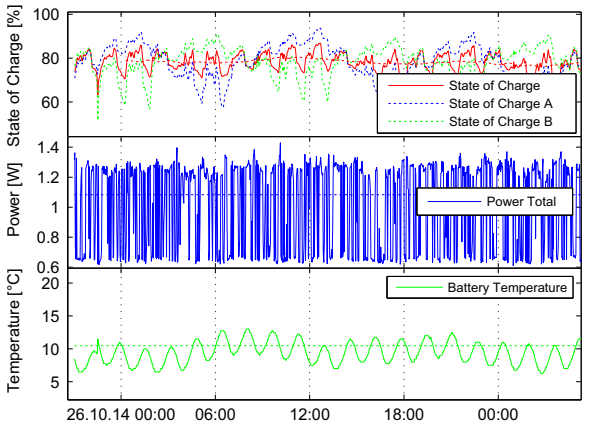


Fig. 5. Power, charge-state and battery temperature recordings during high precision – high power attitude control experiment.

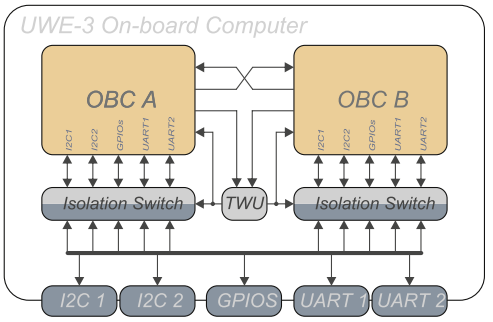


Fig. 6. Block diagram of the redundant low-power onboard computer of UWE-3.

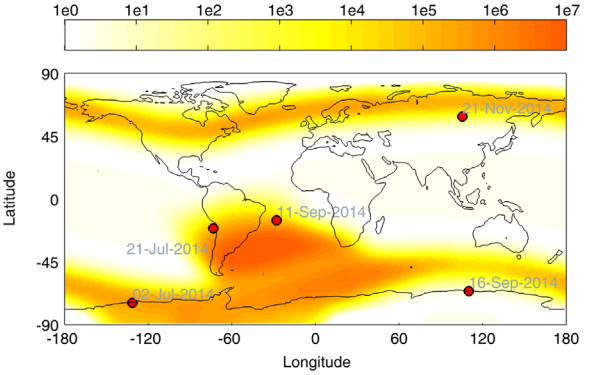


Fig. 7. Single event upsets observed after software update in June 2014, overlaid on AE-8/AP-8 MAX Integral Flux ($cm^{-2}\,s^{-1}$) for the UWE-3 orbit.

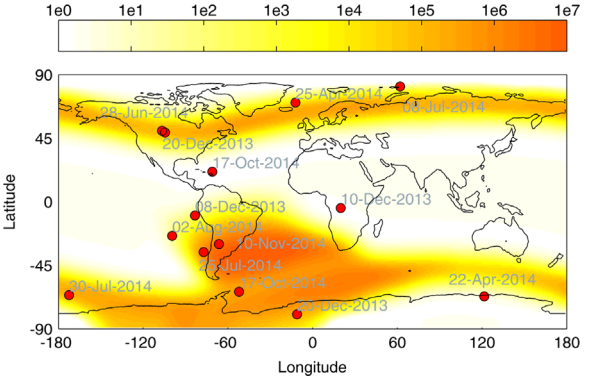


Fig. 8. Automatic switch-over recovery events, overlaid on AE-8/AP-8 MAX Integral Flux ($cm^{-2}\,s^{-1}$) for the UWE-3 orbit.

assembled. Standardized connector interfaces replace here the traditional harness.

In order to provide reliability despite mentioned constraints related to limited budgets on miniature spacecraft, fault-tolerance is mainly accomplished by redundancy and failure detection, isolation, and recovery techniques. As also addressed by Shirasaka and Nakasuka [14] it is assumed that most failures are not inherently destructive such that they can be recovered for example by power cycles as long as key components remain operational to ensure that advanced recovery procedures can be initiated. Thus, at least most crucial subsystems of UWE-3 such as the onboard computer, the electrical power system and the communication system provide in-system redundancy at optimized performance and power consumption.

The UWE-3 bus features a dual-redundant low power onboard computer (OBC), a redundant and distributed electrical power system (EPS), a redundant UHF communication system with separate monopole antennas (COMM) and an attitude determination and control system (ADCS) being capable of operating continuously on the power-constrained pico-satellite.

UWE-3 was launched on Nov. 21st at 07:10:11 UTC on board a Dnepr rocket. Within the first months of operations all subsystems and redundancies have been tested, both antennas have been successfully deployed and

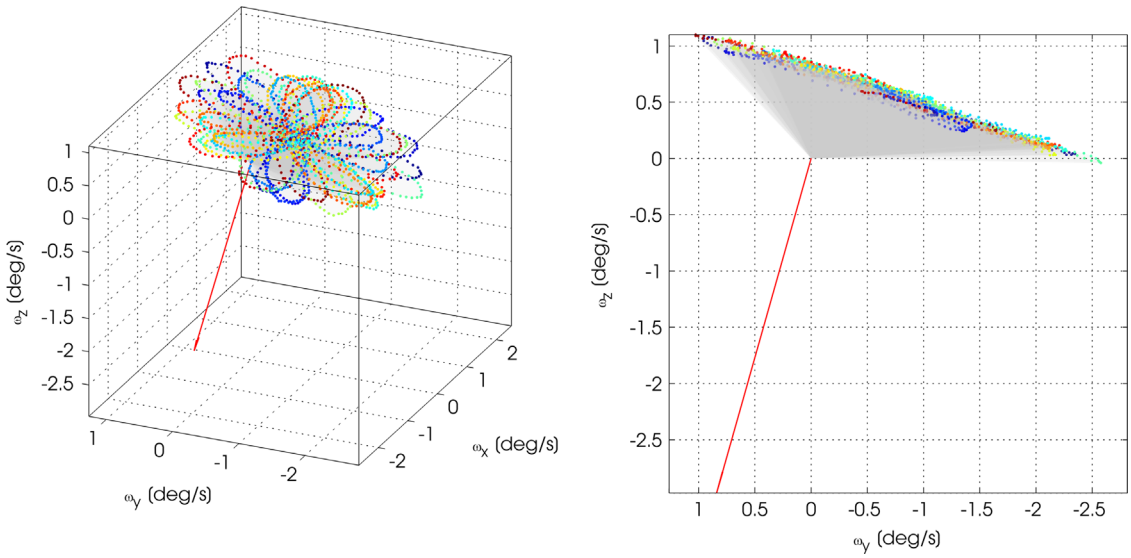


Fig. 9. Rate vector in Body coordinates. The color code is the elapsed time. Estimated magnetic moment is shown as red arrow. (For interpretation of the references to color in this figure legend, the reader is referred to the web version of this article.)

communication with ground could be established with both radio configurations. First results from UWE-3 early operations and first attitude determination and control experiments have been published in [1] and [3]. In the following sections a more detailed overview about the satellites performance during its first year in orbit is presented.

2.1. Temperature and power

From beginning of operations UWE-3 has shown an excellent health state. Measured extreme temperatures on the outer panel structure vary within ± 30 °C with a mean of $+4$ °C in the first months. The maximum temperature rate observed remains within ± 3 K/min. As expected, the most moderate temperature environment is inside the MLI insulated battery case, keeping the Lithium-Ion batteries within 0 °C and $+10$ °C during nominal operations. The orbital temperature variation inside the battery case is in the order of 5 K.

As can be seen in Fig. 3, despite temporal peaks due to increased power consumption of the satellite, the battery mean temperatures show also a seasonal variation. However, as the temperature remains always well above 0 °C even without active heating, the included battery heaters have not been used so far. These results basically reflect our assumptions and observations made during thermal vacuum test campaign prior to launch when the satellite has been exposed to thermal cycles within ± 40 °C as depicted in Fig. 4.

Being launched with fully charged batteries UWE-3 converged to its expected power balance within several hours after orbit insertion. During nominal operations the satellite consumes about 320 mW in total. This allows to maintain a stable charge state well above 90 percent of the battery capacity which reflects our estimations prior to launch. No degradation can be identified during the first year in orbit.

Further long-term in-orbit performance tests could demonstrate stable provision of 1.1 W orbit average power (see Fig. 5), which leaves more than 70% verified margin in the satellites nominal power budget for energy demanding attitude control experiments. Nevertheless, provision of higher orbit average power might be possible in low Earth orbit such that further experiments and optimizations are expedient in preparation for future missions.

2.2. Onboard computer

Due to its central role the design of the UWE-3 onboard computer, as described in more detail in [4], enhances reliability by implementing two redundant processing units on a single subsystem board. As the core module is optimized for housekeeping and basic operations the design employs ultra-low power microcontrollers as processing units. Thus, the redundant system consumes less than 10 mW in nominal operation. Besides advances in energy efficiency, the utilization of microcontrollers with task-optimized processing capabilities and clock frequency naturally reduces the target for radiation induced SEUs or SETs as compared to more complex soft- and hardware setups. As microcontrollers usually allow code execution from flash memory the design further avoids the need for bootloading and code execution from RAM which provides enhanced robustness regarding critical SEUs in the code section.

As shown in Fig. 6 the core module realizes a warm-backup scheme to be able to automatically recover from failure conditions by initiating a fail-over to the redundant unit without the need for manual interaction. This procedure is controlled by an independent toggle watchdog unit (TWU) being responsible for proper reset and activation of the redundant hardware. A data cross-connection between the redundant devices further enables mutual aid, up to complete mutual re-configuration. Thus, software based EDAC algorithms on the active unit can identify the fault and re-initialize the inactive device if required.

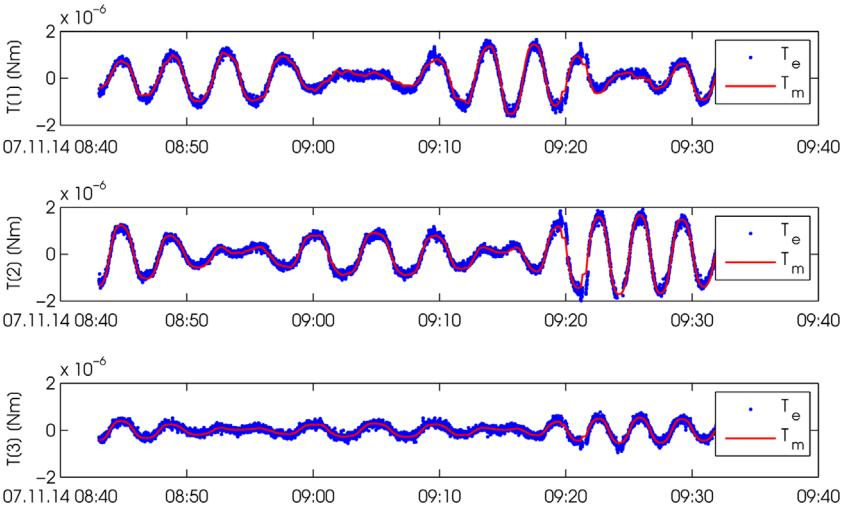


Fig. 10. Torques acting upon the satellite in *x*-, *y*-, and *z*-direction respectively. In blue, the total torque derived from the satellite's spin rate is shown. The torque produced by the residual magnetic dipole at every instance is shown as a red line. (For interpretation of the references to color in this figure legend, the reader is referred to the web version of this article.)

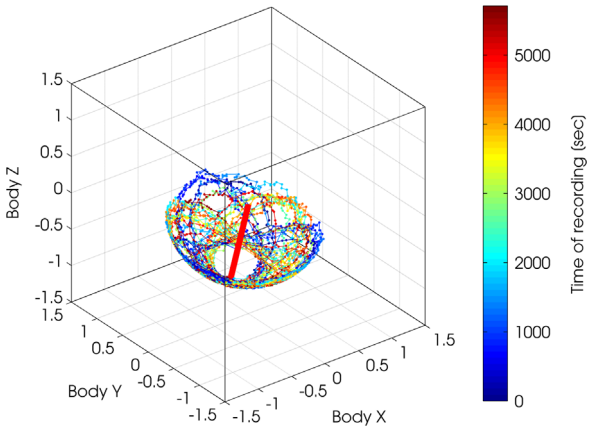


Fig. 11. Magnetic field vector in Body coordinates, the red arrow indicates the estimated magnetic dipole. (For interpretation of the references to color in this figure legend, the reader is referred to the web version of this article.)

Beside automated warm-backup, the redundancy scheme supports fail-safe in-orbit software updates which has been successfully demonstrated after the first six month of operation. In June 2014, a binary image of an extended onboard software has been uploaded to the satellite's file system and subsequently flashed to the redundant OBC by the current active device. After updating the remote flash memory via the microcontroller's JTAG/EEM cross connection, the remote code section has been verified before manual switch-over to the upgraded system. In the case of an unexpected malfunction, the TWU would have initiated a fail-over to the intact device and the initial configuration of the updated device could have been recovered easily.

Several radiation-induced failures have been observed in the redundant on-board computer during its first year of operation. The SEU rate observed in a 8 kB region of unused RAM is in the order of 1 upset per month. Various fault states of the active processing unit were recovered by automated fail-over to the redundant processing unit, thus ensuring continuous operation without significant interruptions. No direct correlation of events with Solar activity could be identified [3]. However, as indicated in Figs. 7 and 8, the majority of events have been observed inside the orbit's main radiation environment within the van Allen belts and the South Atlantic Anomaly.

2.3. Attitude determination and control

UWE-3 has been launched to demonstrate real-time attitude determination and to achieve first attitude control for the UWE platform. The former has been accomplished, its performance characterized and the results have been published in [1] and [3]. While working to further improve the attitude estimation capabilities of the satellite, the focus has shifted towards active attitude control. Preceding work comprises the satellite's active detumbling in Dec. 2013 and functionality tests of the reaction wheel. Furthermore, the presence of a residual magnetic dipole has been found, which directly affects attitude control. In the following sections the approach to attitude control of UWE-3 as well as results of experiments with a spin controller are described.

2.3.1. Residual magnetic moment

By identifying certain features in the natural movement of the satellite, it became apparent that its rotation is dominated by the interaction of the Earth's magnetic field and an inherent residual magnetic dipole μ within the satellite. In order to prepare attitude control for absolute pointing, it was essential to estimate the magnetic dipole's orientation and strength.

High resolution recordings of the satellite's rotational rate show that the rate vector's trace lies in a plane, such that its changes also lie in the same plane (see Fig. 9). Assuming that the torque due to the magnetic dipole T_μ is the only external torque acting on the satellite, Euler's equation simplifies to

$$T_{\text{ext}} \stackrel{!}{=} T_\mu = \mu \times B = \mathrm{I}\dot{\omega} + \omega \times (\mathrm{I}\omega) \approx \mathrm{I}\dot{\omega},$$

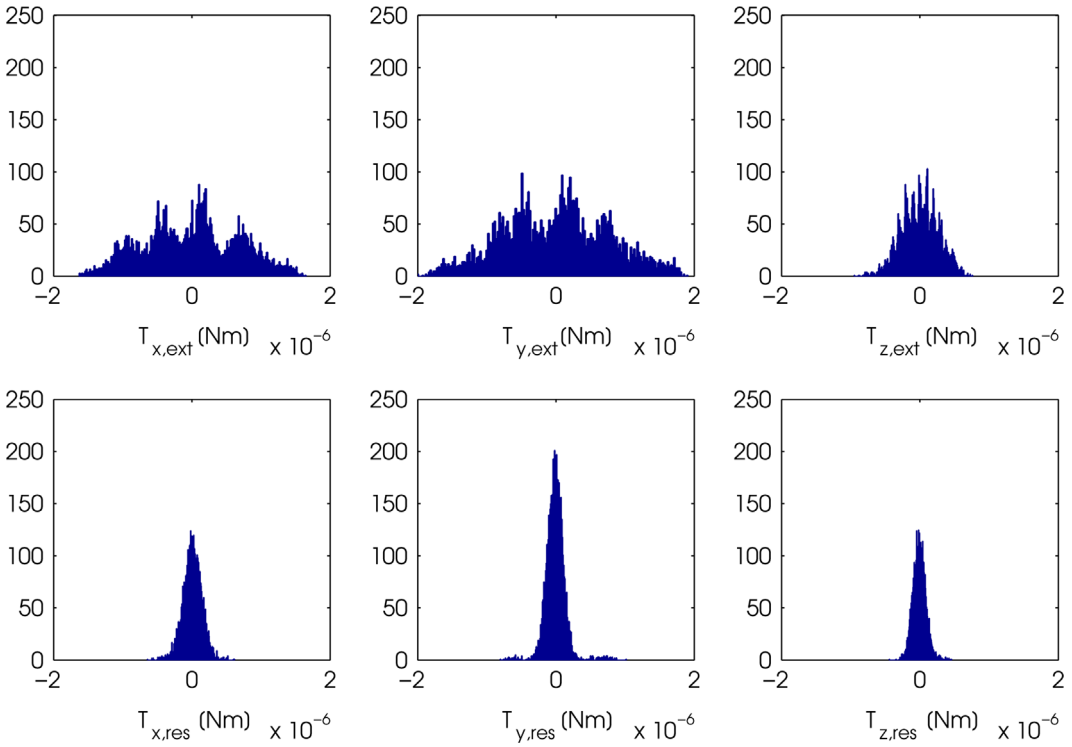


Fig. 12. Histogram of the torque acting on the satellite T_{ext} (top) and which cannot be explained by the consideration of a magnetic dipole T_{res} (bottom).

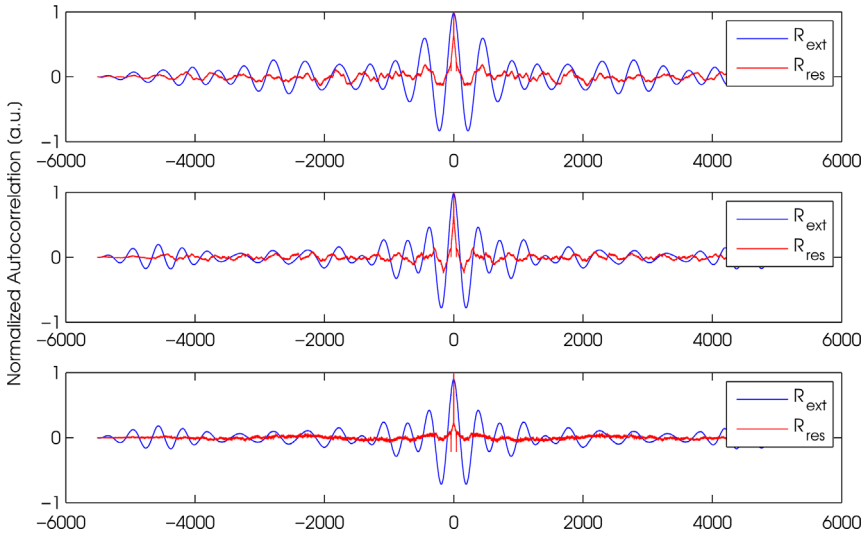


Fig. 13. Normalized autocorrelation functions of T_{ext} and T_{res}.

for small rotation rates and an inertia tensor close to a scalar matrix. Thus, for these cases μ is perpendicular to the plane spanned by the rotation vector.

In order to find the magnetic dipole the differential rotation rate $\dot{\omega}$ was numerically found and inserted into Euler's equation together with an estimated inertia tensor I and ω to give an expected torque T_{ext} in Body coordinates. With simultaneous recordings of the magnetic field B in Body coordinates, a magnetic torque $T_\mu = \mu \times B$ can be calculated for any constant μ. Using the error function $E = \sum (T_{ext} - T_\mu)^2$, a magnetic dipole could be found that produces a torque which matches the experienced torque as shown in Fig. 10.

The estimated magnetic dipole was found using several recordings to be on the order of $\mu = [-0.001, +0.012, -0.045] \pm 0.001$ Am^2. The direction of the dipole is shown in Fig. 9 where its perpendicularity onto the plane of ω is clearly visible. Furthermore, the magnetic

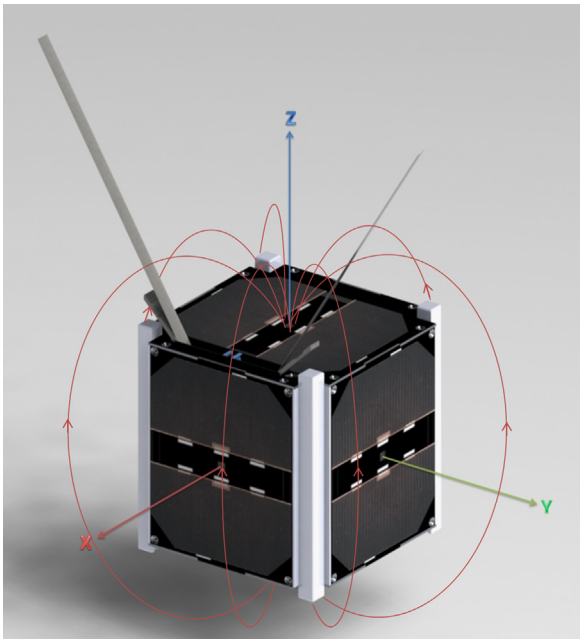


Fig. 14. Visualization of the magnetic dipole in the satellite's Body reference frame. The antennas have been identified as the most probable cause.

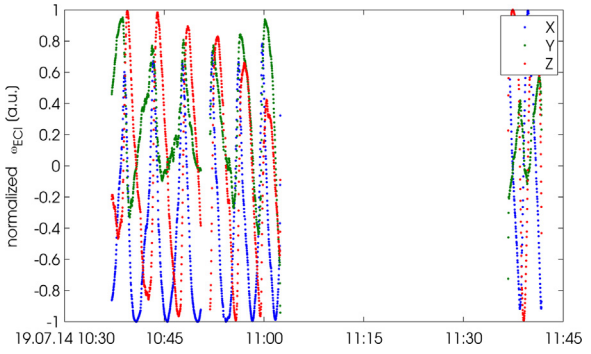


Fig. 15. Angular velocity direction in ECI coordinates during a slow rotation of about 1 deg/s. The rate vector changes direction in ECI coordinates throughout the orbit, indicating that an external torque dominates the satellite's motion.

field in Body coordinates naturally swings about this dipole, which is shown exemplarily in Fig. 11.

The consideration of a residual magnetic dipole explains a major part of the measured torque acting upon the satellite. In fact, an R^2 value of 0.906 can be found when considering the torque explained by the magnetic dipole as fitting curve. However, it became of interest on how well it can explain the satellite's dynamical behavior.

To do so, the residual torque $T_{res} = T_{ext} - T_{\mu}$ that remains after subtracting the torque due to the magnetic dipole from the measured external torque T_{ext} is analyzed. In Fig. 12 the histograms of the external and residual torques are shown for each component, where the almost Gaussian distribution of the residual torque is apparent. The RMS of the residual torque is 79.8% less than that of the torque acting on the satellite.

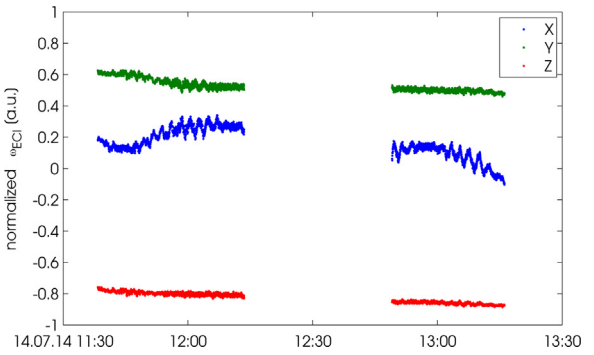


Fig. 16. Angular velocity direction in ECI coordinates during a fast rotation of about 80 deg/s. The rate vector retains its direction in ECI coordinates throughout the orbit, indicating that the satellite's motion is spin stabilized.

In order to check the residual torque for systematic behavior, the normalized autocorrelation R of the torque is computed and shown in Fig. 13. It can be seen, that the torque acting on the satellite T_{ext} shows a significant autocorrelation. The residual torque however has a quite small autocorrelation signal, which confirms the hypothesis that it is primarily white uncorrelated noise.

Nevertheless, there is a small systematic component persistent in the signal, causing the autocorrelation to have small side lobes and therefore to differ from a delta function at position zero. This component within the unexplained residual torque can have different sources out of which minor miscalibrations of the sensors are expected to have the largest influence. However, this contribution is comparably small with respect to the explained dominating influence of the static magnetic dipole.

The dipole mainly lies in the satellite's z-axis, as shown in Fig. 14, which limits the list of potential causes to internal magnetic fields in the batteries, the reaction wheel and the satellite's antennas. During ground-testing with the engineering model, the reaction wheel and batteries could be eliminated which leaves the strong assumption that the antennas, made out of stainless steel, have been magnetized.

Since the dipole is in the same order of magnitude as the one produced by the magnetic torquers, measures to demagnetize the dipole have been investigated, ranging from applying a constant magnetic field in its opposite direction using the torquers, to fast and random magnetic fields. Unfortunately, none of the experiments could significantly change the residual magnetic dipole.

However, precise attitude control appears feasible taking spin-stabilization into account. During an experiment with very high rotational speeds of up to 90 deg/s, the satellite's stability against the magnetic dipole became apparent. This is shown in Fig. 15 and Fig. 16, where the satellite's angular velocity direction in ECI coordinates is plotted. In Fig. 15 the satellite rotates slowly at about 1 deg/s, while the rotation vector in ECI coordinates changes direction due to the influence of the magnetic dipole torque.

In Fig. 16 the satellite spins at about 80 deg/s which stabilizes the satellite, such that its rotation vector in ECI coordinates shows only minor changes in direction over

Table 1
Deviations of sensor measurements from predicted reference models while spinning at 80 deg/s.

Deviation of measurements from reference magnetic vector RMS:	2.9 deg
Deviation of measurements from reference sun vector RMS:	9.6 deg

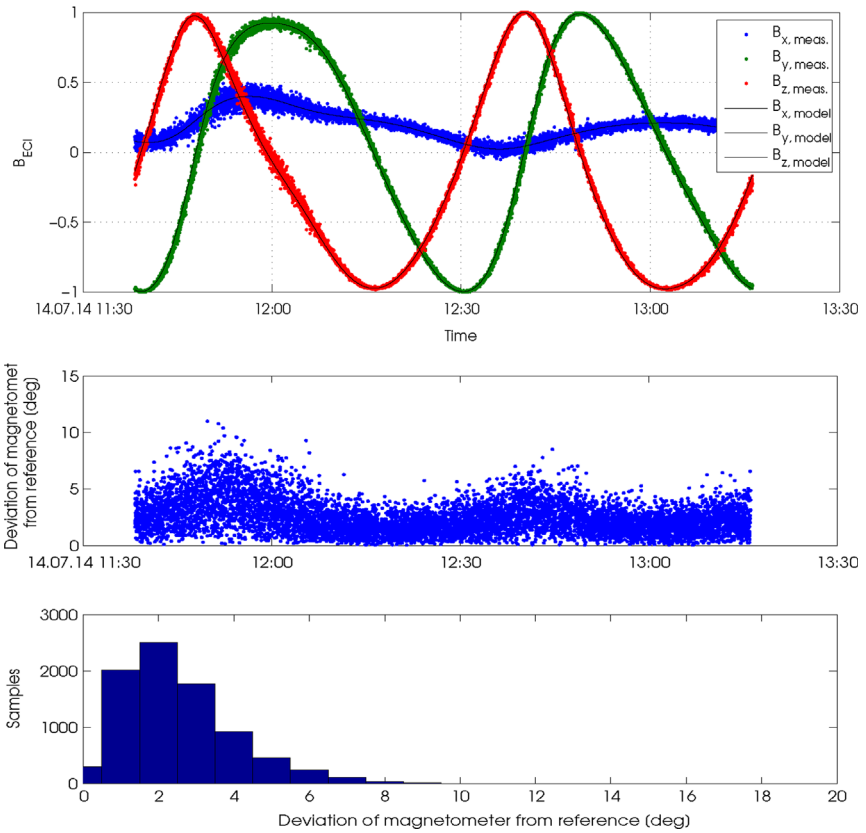


Fig. 17. Magnetic Field vector in ECI coordinates compared to the IGRF model.

the course of one orbit. During eclipse the attitude estimation is not precise enough, such that the gyroscopic rate cannot be transformed into ECI coordinates and therefore no data points are shown for this period.

2.3.2. High rotation rate attitude determination

Spin-stabilized attitude control poses the requirement on the attitude determination system to be capable of estimating the attitude even at high rotational rates. Especially for CubeSat systems employing low power microcontrollers as computational platform this requirement is not easily fulfilled. Very accurate timing of the sensors' measurements as well as efficient algorithms are necessary to have a reliable attitude estimation at high rotational speeds.

The UWE-3 attitude determination has previously been characterized [1] using the estimated orientation and transferring the measurements into the ECI frame. The angular difference between the reference models and the measurements gives an estimate of the attitude determination accuracy, still containing the sensors' noise and therefore serving as a worst case estimate. It was previously found to be on the order of 2.4 deg and 6.9 deg for the magnetic field and the sun-sensor measurements, respectively (RMS deviation from reference data).

Using the same analysis on a recording during which the satellite was spinning at 80 deg/s with the rate vector being $\omega = [73, -2, -32]$ deg/s, the attitude determination accuracy is given in Table 1 and the results are also shown in Fig. 17 and Fig. 18. The deviations are slightly increased compared to the case of a slowly spinning satellite. Especially for the sun-sensors this increase might be caused by small uncertainties in timing of the sensors.

However, it should be noted that these deviations still contain the sensor's internal noise. The sun-sensors have an accuracy according to their datasheet, of ± 5 deg and the magnetometers have been shown during tests to be precise to better than 3 deg.

2.3.3. Detumbling

Another requirement for safe spin-stabilized control is that the ADCS is capable of slowing down high spin rates

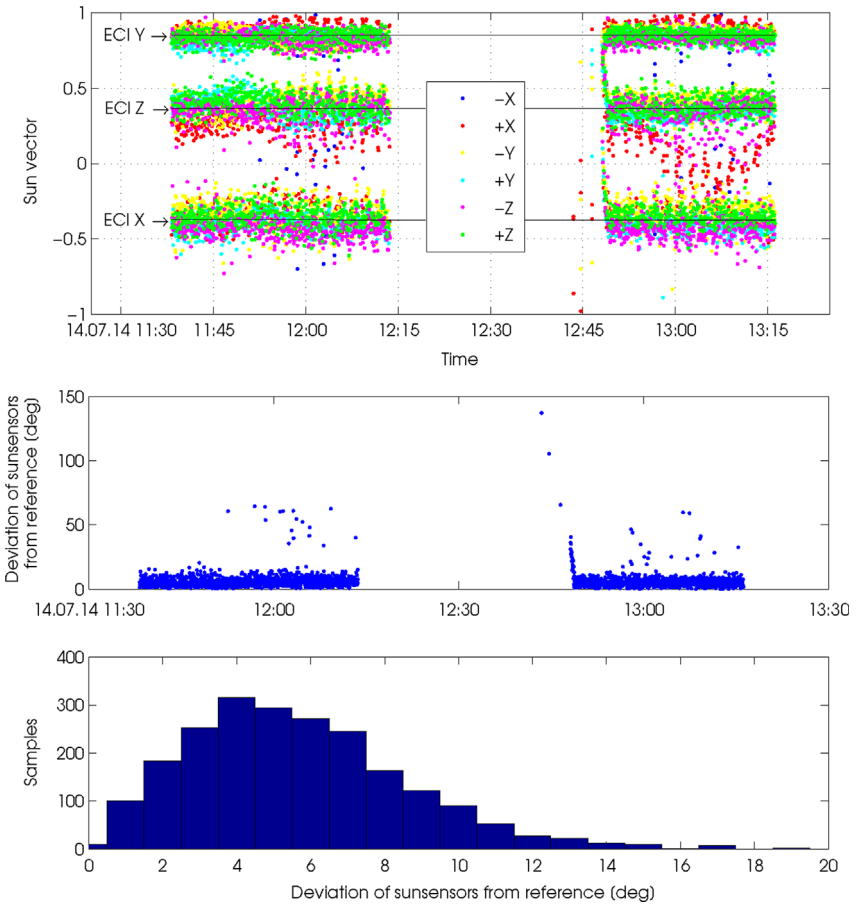


Fig. 18. Sun vector in ECI coordinates compared to the sun model.

reliably. Its effectiveness has already been shown in Dec. 2013 during the initial detumbling [1]. Fig. 19 shows the detumbling process from an initial spin rate of 80 deg/s, which was completed in about 40 min. Shown in Fig. 20 is the corresponding 3-D representation of the rotation rate vector. From this it becomes visible, that the ADCS is capable of slowing down the satellite even at very high spin rates.

Furthermore, the algorithm stabilizes the satellite with an RMS of 0.7353 deg/s about zero (0.3968, 0.4953, 0.3714 deg/s in *x*, *y*, *z*-components respectively).

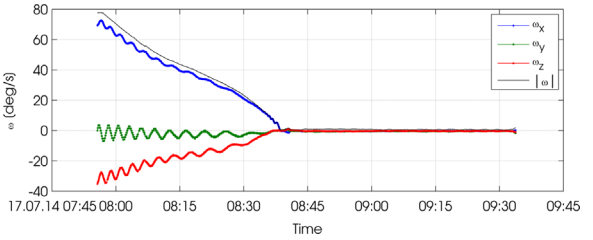


Fig. 19. Rate vector during detumbling from about 80 deg/s. The satellite reaches its stable state after 40 min and remains with an RMS of 0.7353 deg/s about zero afterwards.

2.3.4. *Spin-z controller*

Spinning up the satellite about one defined axis precisely has been the next step towards spin-stabilized attitude control. In Fig. 21 an experiment is shown during which the satellite was spun up from an initial set-point of −10 deg/s about its *z*-axis to +10 deg/s about its *z*-axis. The controller intends to minimize the rotation about the *x*- and *y*-axes simultaneously.

The controller is able to perform the transition of 20 deg/s about the *z*-axis within 18 min, after which it retains the intended spin rates. The corresponding 3-D trace of the angular velocity is shown in Fig. 22.

However, there are two periods during which the *y*-axis rate significantly moves away from its set-value (Fig. 23). A correlation with the measured magnetic field reveals that during this period the magnetic field along the satellite's *z*-axis vanishes (i.e. the magnetic field lies within the *xy*-plane) which affects efficient torque production in the *xy*-plane. This effect is even more prevailing during an earlier experiment, shown in Fig. 24, in which the controller was active for three consecutive orbits.

Apart from these deviations the controller retains an RMS of [0.1196, 0.25077, 0.0892] deg/s for the *x*-, *y*-, and *z*-axis about their set-points respectively.

The successful test of this spin-*z* controller has confirmed the effectivity of a stepwise approach to spin stabilized attitude control. A controller allowing an arbitrary spin axis

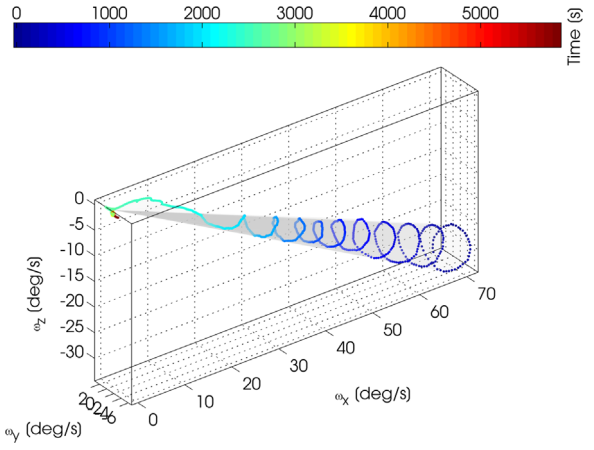


Fig. 20. 3-D representation of the angular rate vector trace during detumbling.

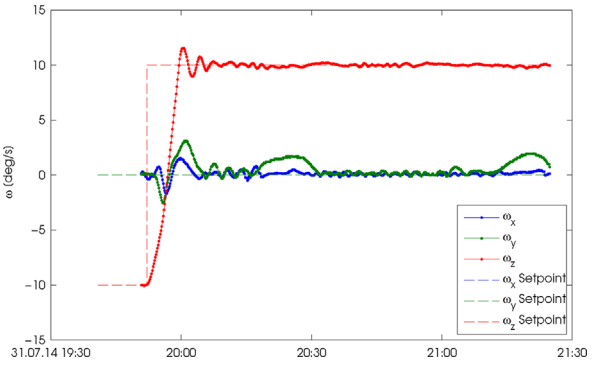


Fig. 21. Angular rate vector during spin-up to setpoint 10 deg/s from an initial setpoint of −10 deg/s about the Body z-axis.

is in preparation, targeting a spin axis perpendicular to the residual dipole such that effects of the latter onto the satellite's attitude can be minimized. Furthermore, the improved controller shall keep the spin axis constant in ECI coordinates, such that sun-pointing for instance can be achieved.

3. Satellite operations

In order to enable the communication with the UWE-3 satellite, the University of Wuerzburg UHF ground station is equipped with an Icom IC910 transceiver, an SPS tracker TNC unit, a YAESU G5500 rotator and a liftable cross yagi UHF antenna fixed on the roof of the department (see Fig. 25).

3.1. Automated groundstation operations

A typical operations workday of the UWE team members begins at 7:00 UTC and ends at 16:00 UTC (summer time). During this period three to four satellite overpasses can be used to perform operations. However, there are another three to four overpasses during the night period (20:00–01:00 UTC) such that a remote accessibility of the university's ground station was mandatory to enable operations from the outside.

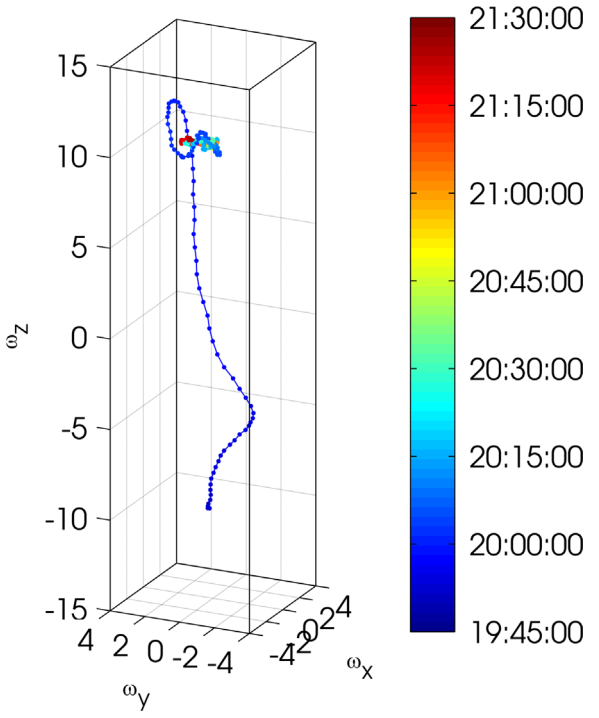


Fig. 22. 3-D representation of the angular rate vector trace during a spin-up experiment to setpoint [0, 0, 10] deg/s.

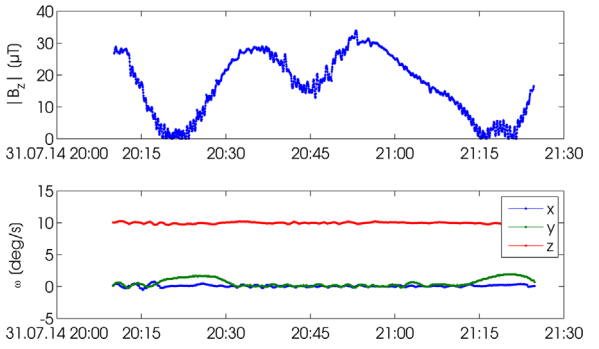


Fig. 23. The top shows the magnetic field's Body *Z*-component throughout the spin-*z* experiment whereas the bottom graph shows the angular rate vector. Note that the periods in which ω_y deviates significantly from its set-point coincide with very low magnetic field strengths in the Body *Z*-direction.

3.1.1. Remote access to groundstation

The ground segment software is build up of two main parts: ground station server and operations client. The server is responsible for proper hardware setup (e.g. antenna orientation, transceiver) and is able to broadcast received satellite packets along the connected clients. It transmits client packets (e.g. tele commands, requests) via the radio and synchronizes all clients among themselves, providing the operator an insight into the actions of his collaborators. The client software can be executed on arbitrary workstations presupposed that the server is reachable within the available network. Typically multiple

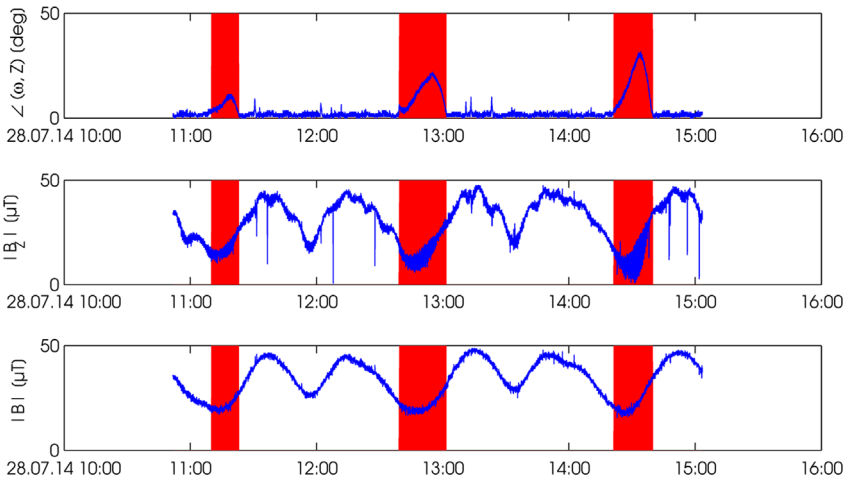


Fig. 24. Deviations from the set spin-axis (shown in the top graph in degree) occur, when the magnetic field in the Body *Z* axis vanishes. Marked in red are time intervals during which the spin axis deviates significantly from its set-point which occurs one per orbit. (For interpretation of the references to color in this figure legend, the reader is referred to the web version of this article.)



Fig. 25. UHF Cross yagi ground station antenna on top of the computer science department.

workstations are simultaneously engaged during operations.

3.1.2. *Automated operations*

The commanding interface has a wide functional range such as file system operations, ADCS controlling, script execution, etc. During the initial operations phase all actions had to be initiated manually as soon as the satellite was within range. During the night time many overpasses remained unused.

In order to optimize the utilization of contact times, satellite operations had to be automatized. That is to enable a predefinition of all necessary operation tasks, which are automatically executed as soon as the desired satellite is reachable. Furthermore, each task can be executed periodically – e.g. daily or during every overpass. Based on these requirements an operations scheduler has been implemented. To allow automated operations without connected clients, the scheduler is located on the ground station server. Connected clients can view all propagated overpasses (also for multiple satellites) and scheduled operations in a scheduler view (see Fig. 28, Section 3).

The server has been extensively updated to fulfill the requirements of the scheduler. That is fast orbit prediction of a single or multiple satellites, rapid detection of instantaneous hardware settings, straightforward exchangeability of the hardware components (e.g. for debug purposes).

All software components are implemented as modules with connectable ports for live data flow modifications. Each module is designed to fulfill one particular task, such as orbit propagation, activating auto operations jobs, radio/TNC/antenna control. The current activity of all components and the data flow are observable live in the GUI in which modules can be added, removed or modified during runtime (see Fig. 28, Section 4).

With the operations scheduler automated uplink performance tests could be carried out (see Section 3.2). Further, file uplink and downlink tasks have been implemented

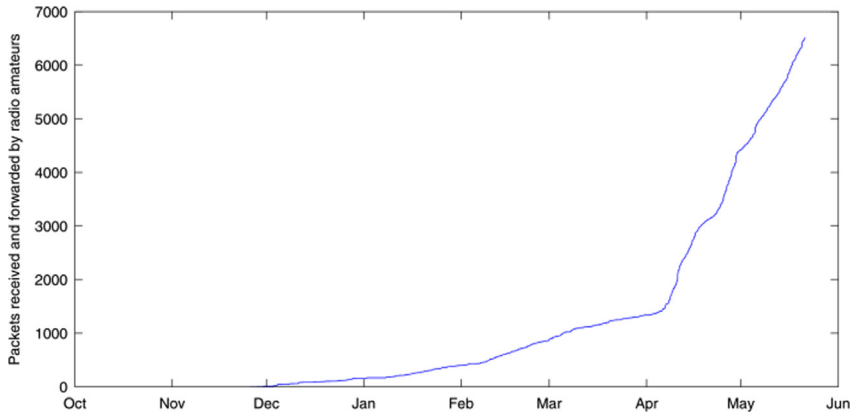


Fig. 26. Number of UWE-3 packets submitted by radio amateurs.

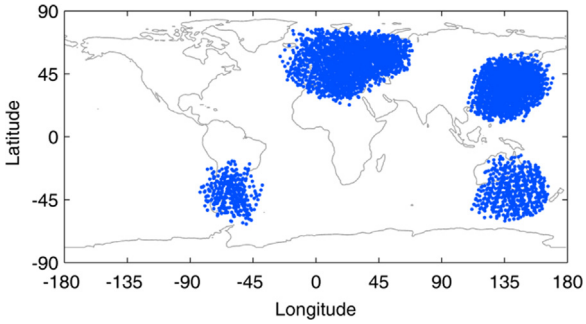


Fig. 27. Receive locations of UWE-3 packets submitted by radio amateurs.

allowing to automatically transfer large data files from ground to the satellite and vice versa. By using the uplink task a new software image has been automatically uploaded to UWE-3 onboard computer within several night passes.

3.1.3. *Live-injection of remotely received data*

A further downlink yield improvement was achieved by involving radio amateurs. Many radio amateurs have supported the UWE-3 team by forwarding received satellite packets via e-mail. To accelerate the data submission a web server was introduced enabling injection of externally received packets. This way the UWE-3 team is able to receive packets even if the satellite is not within range. As it can be seen in Fig. 26, the amount of remotely received packets was drastically increased after the web server kick-off in April 2014. The location of UWE-3 during packet reception is shown in Fig. 27.

3.1.4. *Multiple satellite tracking*

In order to test the task scheduler's ability of multiple satellite tracking, UNISAT-6 from GAUSS-Team was added as an additional target. In case of simultaneous reachability of multiple targets, the one with the higher priority is privileged. During every overpass of UNISAT-6, a listener task is activated such that all received packets can be saved and forwarded to a remote server. For this purpose the GAUSS team has established a web server with the same interface as used for UWE-3 external packet injection. Hereby the new downlink-only ground station network approach has been successfully verified. Every ground station which is capable of multiple satellite tracking can be easily integrated into this network. To also share the uplink capabilities of a ground station, a joint project with other universities in Germany is currently in progress.

3.2. *Analysis of global Interferences in amateur radio band*

UWE-3 employs two fully redundant UHF transceivers with separate omnidirectional monopole antennas operating in the 70 cm amateur radio band (435.000–438.000 MHz). While the satellite's tranceivers provide about 1 W transmit power, the university's groundstation operates at 70 W on a 3 m cross-yagi antenna with 14 dB gain.

From beginning on the downlink quality from the satellite to ground was excellent, showing high signal strenghts even at low elevations. However, the telecommand uplink was initially difficult with transmission failure rates between 80% and 90%. From beginning of 2014 the uplink quality degraded further, resulting in average failure rates between 90–95%, which could sporadically extend to 98–100% for several passes, while still providing excellent downlink quality.

Both, ground and space borne hardware defects could be excluded from potential failure sources as the problem remained when operating on the redundant devices. The problem has been further analyzed by performing various automated uplink tests. In order to efficiently identify the uplink success rate, short data frames containing a unique id have been frequently uplinked directly to a file in the satellite's flash memory without acknowledgment requests. In the course of the test, parameters such as offsets in antenna pointing or uplink frequency have been altered randomly. After downloading the file, the received frame identifiers could be directly compared with the uplinked frame identifiers to correlate the success rate with instantaneous frequency offset, satellite position, etc. As it can be seen in Fig. 29, a potential frequency drift, e.g. caused by temperature variations at the satellite's receiver, could also be excluded as failure source, as the success rate is not affected by slight frequency deviations. However, it could be identified that the uplink quality significantly changes in

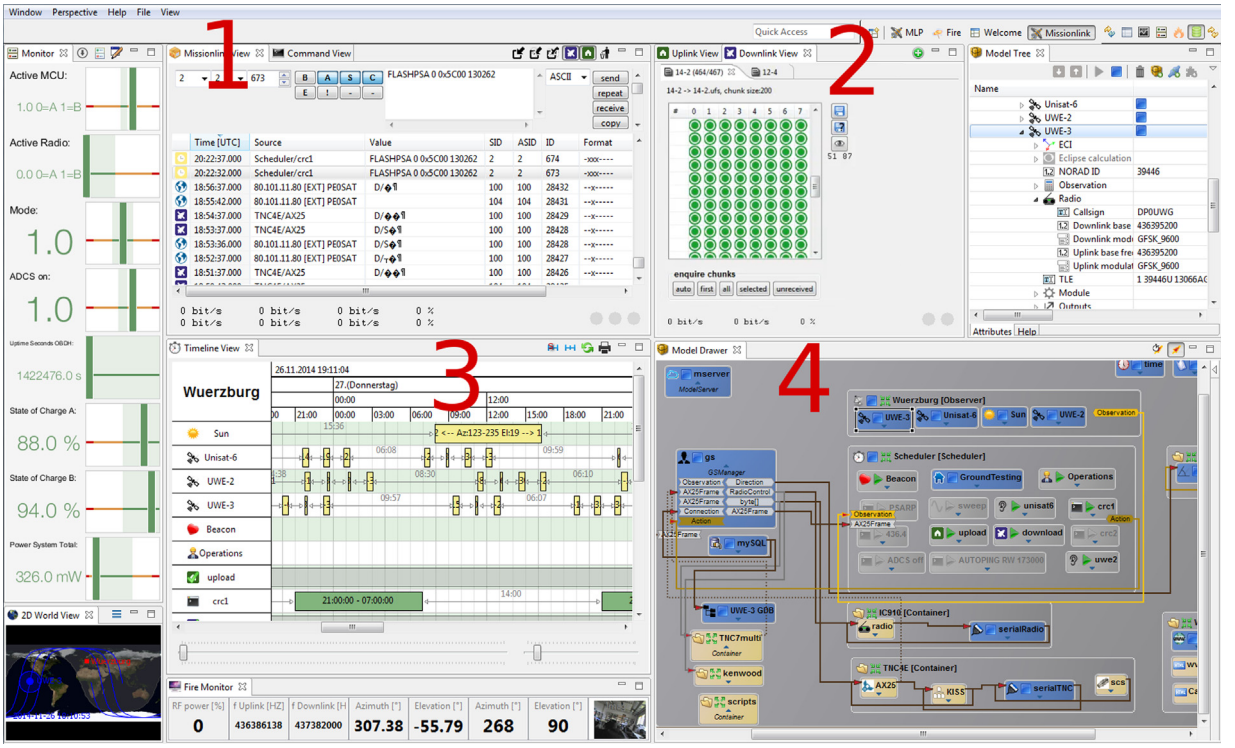


Fig. 28. Screenshot of the client software in action with a packet view (1), uplink/downlink view (2), operations scheduler (3) and remote server software view with dynamic packet visualization (4).

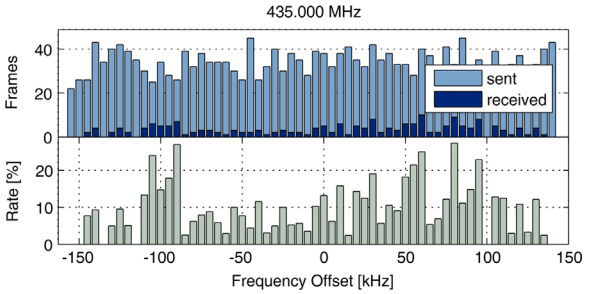


Fig. 29. Exemplary uplink quality analysis based on a ground based frequency sweep around 435.000 MHz ± 150 kHz from 15/16 April 2014.

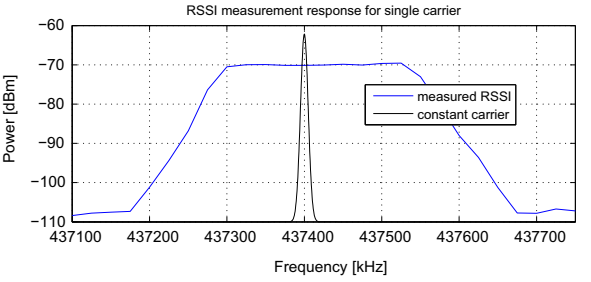


Fig. 30. RSSI [dBm] frequency sweep showing response to a constant carrier signal at 437.400 MHz. C_f=(437.100 MHz, 437.800 MHz, 20 kHz), C_a=(1000 ms, 1, 3).

general within the amateur frequency band and further slightly varies with the satellite's relative location.

Following a trial-and-error search on different frequencies, a good candidate has been found such that the uplink quality could be improved significantly and the satellite operations and experiments could be conducted more efficiently again.

In beginning of June 2014 a software update has been uploaded to one of the redundant onboard-computers of UWE-3. Among other features, the update included several new experiments targeting the analysis of the link quality. In order to further analyze the spatial distribution of in-situ interference levels for the whole amateur radio spectrum, an RSSI frequency sweep experiment has been implemented. The experiment allows to monitor and log measured RSSI noise levels, while automatically scanning over a specified frequency range. Besides start and stop time, the experiment allows to configure target frequency range and scan interval $C_f=(f_{start}, f_{stop}, \Delta f_{step})$. Further, the data acquisition can be controlled with parameters $C_a=(t_s, n_b, n_m)$ for RSSI sampling rate t_s, number of averaged samples in a measurement n_b, and number of repeated measurements for a single frequency n_m.

As the on-board radio is used for the RSSI sampling, first the device response to a single carrier has been determined on the engineering model on ground. As can be seen in Fig. 30, the RSSI measurement is sensitive to a range of $f_{base} \pm 110$ kHz when the radio is configured to a specific receive frequency f_{base}.

Fig. 31 shows an in-orbit frequency sweep recording from 15th of June when UWE-3 had a high elevation pass-over in the west of Wuerzburg. Throughout the entire measurement the signal emission from our groundstation has been deactivated. It can be seen that the background noise level

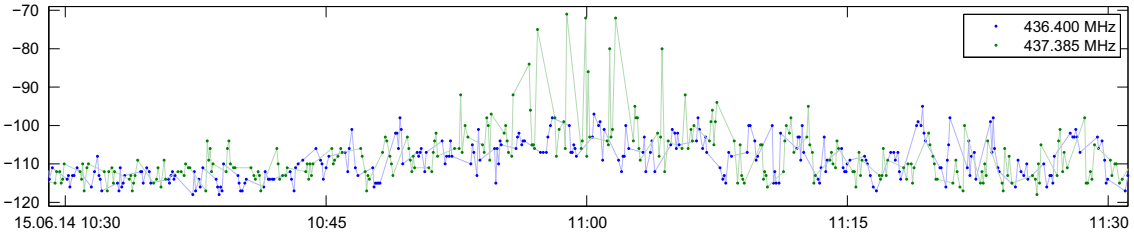


Fig. 31. RSSI noise levels [dBm] measured on-board UWE-3 during a pass over central Europe without groundstation operations in Wuerzburg. C_f=(436.400 MHz, 437.385 MHz, 985 kHz), C_a=(5000 ms, 1, 6).

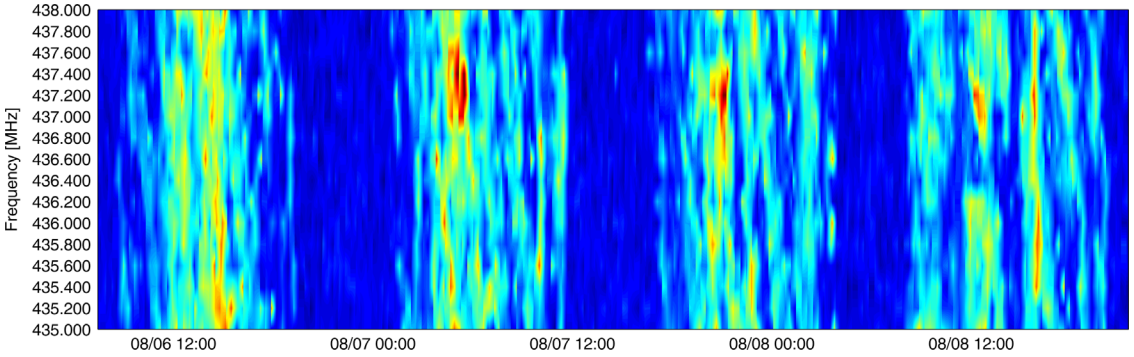


Fig. 32. Extract from the raw RSSI [dBm] measurements over time [UTC]. (Colorbar similar to Fig. 33). C_f=(435.000 MHz, 438.000 MHz, 200 kHz), C_a=(250 ms, 10, 2). (For interpretation of the references to color in this figure legend, the reader is referred to the web version of this article.)

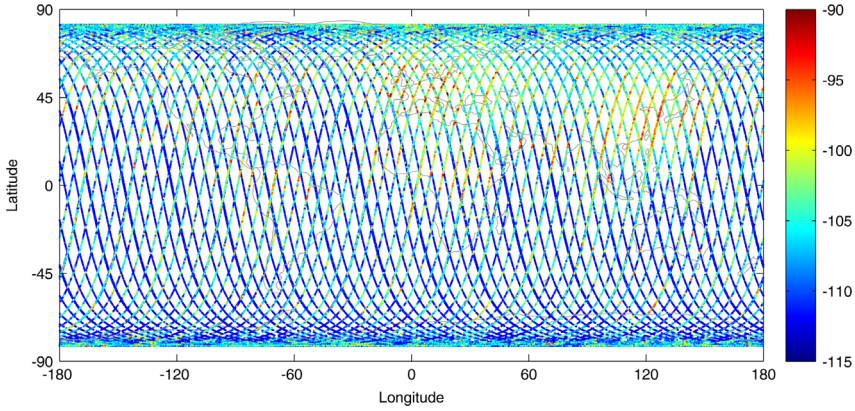


Fig. 33. Orbit coverage of measurement recording. (For interpretation of the references to color in this figure, the reader is referred to the web version of this article.)

increases about 5-10 dB on both observed frequencies when the satellite passes Europe. Further, it can be noticed that the frequency 437.385 MHz is exposed to severe interferences over central Europe with RSSI peak levels ranging up to −70 dBm while the frequency 436.400 MHz is not affected by this source. These measurements could be repeated several times and are representative for the observed time frame in third quarter of 2014.

Described observations lead to further experiments targeting the global spatial distribution of interferences on the entire UHF amateur radio band used for satellite operations. Several frequency sweeps have been recorded in third quarter of 2014, each lasting several days to ensure global coverage. The results discussed in the following are based on measurements recorded between 06.08.2014 and 11.08.2014, and are representative for the performed observations. The recording comprises more than 100.000 data points downloaded from the satellite in a 1.5 MB compressed data file. The measurements have been recorded with the following configuration: C_f=(435.000 MHz, 438.000 MHz, 200 kHz), C_a=(250 ms, 10, 2). In order to ensure the observation of sporadic short interference peaks, a high sampling rate of 250 ms has been chosen. Each recorded measurement represents the average of 10 samples, thus reducing the amount of data produced. Fig. 32 shows the mean RSSI level from an exemplary data set versus base frequency f_{base} and time.

The downloaded measurements have been mapped to their instantaneous sub-satellite points as visualized in

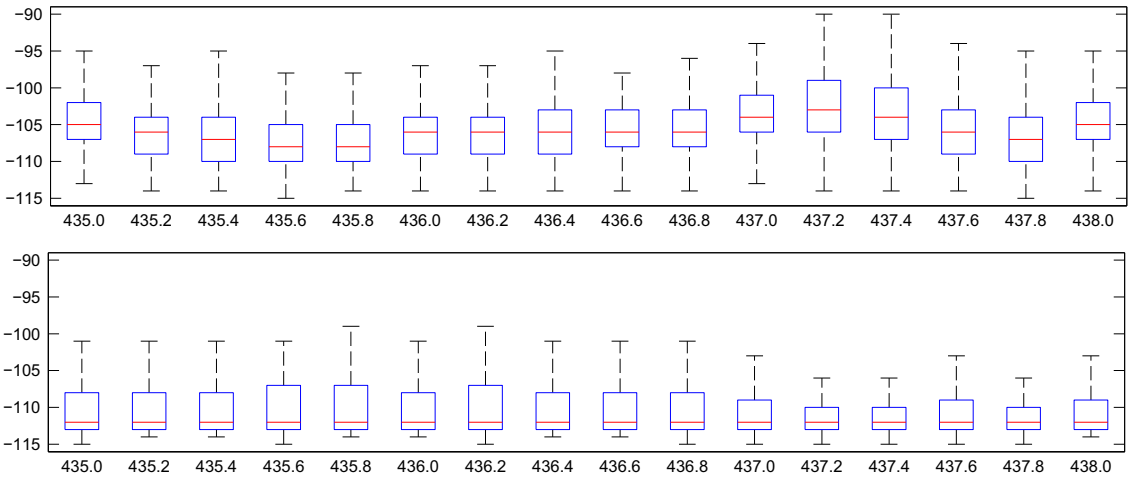


Fig. 34. Average interference statistics for each frequency for Europe centered at groundstation in Würzburg (top) and for a reference without interferences over the pacific (bottom). (Box: first and third quartiles, median of average RSSI [dBm] (10 samples in 2.5 s); Whiskers: data in 1.5 interquartile range).

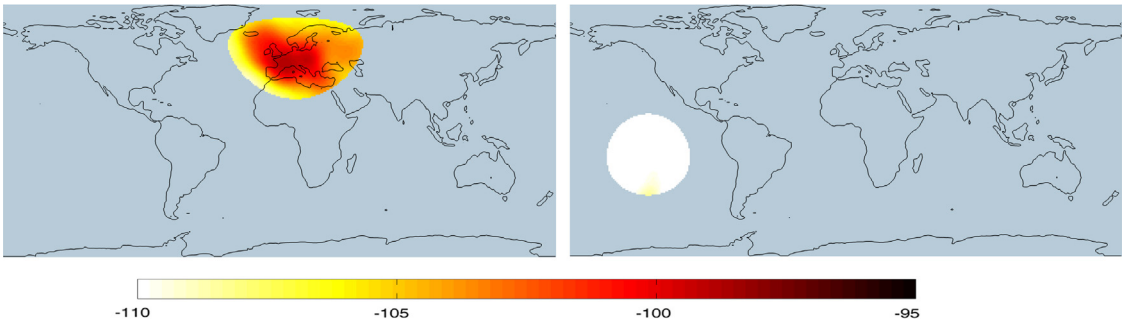


Fig. 35. Reference world plots show RSSI levels [dBm] for 437.400 MHz (corresponding to Fig. 34).

Fig. 33. The recorded data points show sufficient coverage of the entire globe and can properly be used as a grid for spatial interpolation to generate a global interference map for each frequency under investigation. The map interpolation results are shown in Fig. 36. It can be seen that the average interference levels vary significantly with loaction and observed frequency. Especially orbital regions connected to central Europe seem to be affected significantly on a wider frequency band between 437.000 MHz and 437.600 MHz.

In order to express these observation with concrete numbers, a local statistical analysis has been made. For this purpose the measurements have been filtered for specific locations and frequencies in oder to calculate statistical measures such as median and quartiles of the underlying distribution of observed averaged RSSI levels. Fig. 34 depicts the statistical analysis for two different regions. The first region is centered around the sphere of influence of our groundstation in Wuerzburg. The second region serves as an undisturbed reference with a selected region of similar size located somewhere in the south pacific with the same range (see Fig. 35).

Again, the plots clearly show the noise dependancy in location and especially frequency within the radio amateur band, but it has to be pointed out that the underlying data points represent an average of 10 RSSI samples already. Therefore, the extreme interference levels as present in Fig. 31 are not directly visible anymore in terms of their real outlying value. However, it is ensured that these peaks contribute to the statistics such that the different frequencies can be compared with each other for frequency selection.

The results reflect our experiences when operating UWE-3 during the first six month after launch. They further underline the importance of proper freqency selection for satellites using the amateur radio bands. Moreover, the results emphasize the requirement for in-orbit frequency re-configuration to be able to react to changes of inevitable global interferences caused for example by military space surveillance radars.

4. Conclusions

Pico-satellite formations offer excellent potential for efficient applications in Earth observation and telecommunication missions. Essential enabling technologies related to modular, flexible system design approaches, to robust on-board data handling systems based on FDIR-techniques, as well as to miniature attitude determination

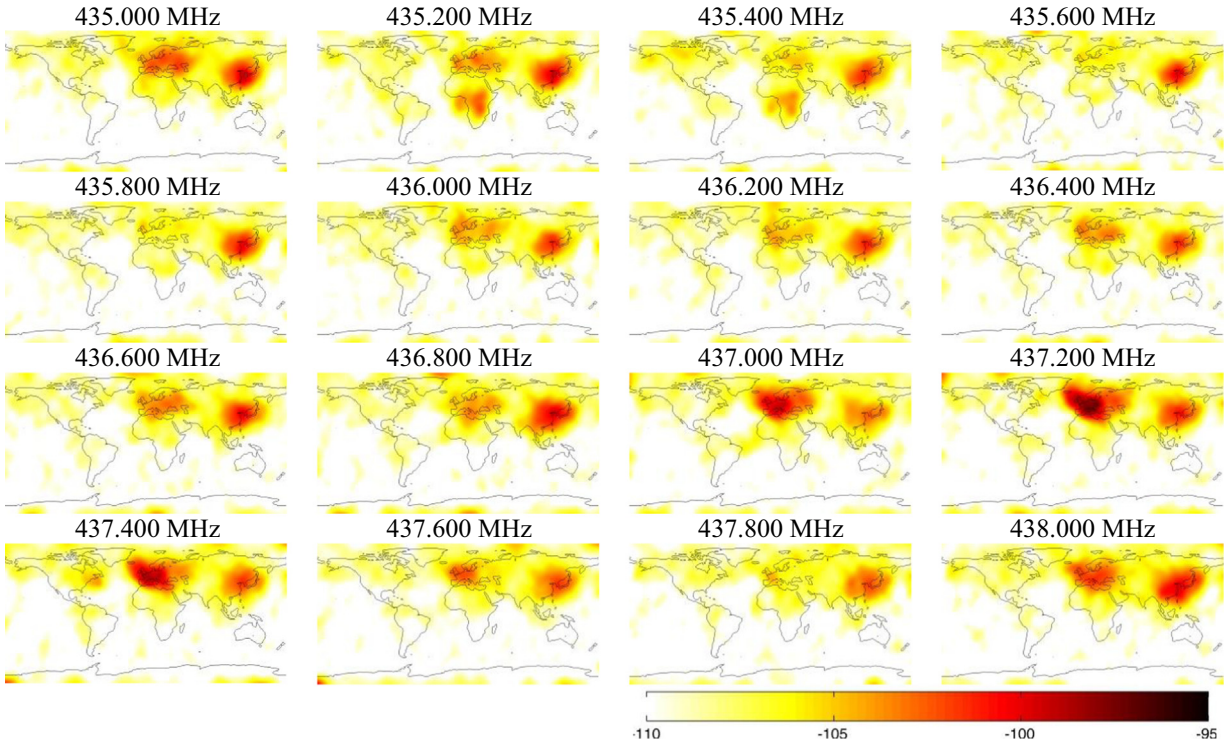


Fig. 36. RSSI [dBm] average interference world plot between 06.08.2014 and 11.08.2014.

and control system implementations are addressed in the UWE-3 project.

The performance of all subsystems and components has successfully been demonstrated in orbit. All redundancies are still active and no performance degradations could be identified during the satellites first year in orbit. Thus, the architecture proofed to constitute a robust base, preparing the subsequent formation demonstration mission “NetSat”.

As an important milestone related to attitude determination and control, it could be shown, that the ADCS is capable of reliably estimating the satellite's attitude, even at high spin rates. An internal residual magnetic moment has been found by analyzing gyroscopic and magnetic measurements. As the magnetic moment dominates the satellite's motion it complicates attitude control. Efficient spin-up and detumbling could be demonstrated, laying ground for further control experiments targeting inertial spin stabilized control.

The UWE-3 software framework for groundstation control simplifies the realization of new automated operation tasks. The groundstation server can be controlled remotely allowing simultaneous access of multiple remote operators. The downlink capabilities of the groundstation are currently shared with other universities. Furthermore, amateur radio operators worldwide are provided with an efficient data injection service.

Temporary uplink quality degradations due to severe interferences in the amateur radio band have been observed. Re-configuration of the uplink frequency could significantly increase performance. In the course of communication link optimizations, the spatial distribution of terrestrial radio interference sources for different frequencies in the amateur radio band has been analyzed in-orbit. Observations underline the need for proper frequency (re-) configuration when operating satellites in the related frequency band, especially from within Europe.

Acknowledgments

The authors appreciated the support for UWE-3 by the German national space agency DLR (Raumfahrt-Agentur des Deutschen Zentrums für Luft- und Raumfahrt e.V.) by funding from the Federal Ministry of Economics and Technology, Germany by approval from German Parliament with reference 50 RU 0901, as well as the European Research Council advanced grant “NetSat”.

References

[1] P. Bangert, S. Busch, K. Schilling, Performance characteristics of the UWE-3 miniature attitude determination and control system, In: Proceedings of the 2nd IAA Conference on Dynamics and Control of Space Systems (DYCOSS), IAA-AAS-DyCoSS2-14-05-07, Rome, 2014.
[2] R. Barza, Y. Aoki, K. Schilling, CubeSat UWE-1 technology tests and in orbit results, In: Proceedings of the 57th International Astronautical Congress Valencia, IAC-06-B5.3.07, 2006.
[3] S. Busch, P. Bangert, K. Schilling, Attitude control demonstration for pico-satellite formation flying by UWE-3, In: Proceedings of the 4S-Symposium, Mallorca, 2014.
[4] S. Busch, K. Schilling, Robust and efficient OBDH core module for the flexible picosatellite bus UWE-3, in: Proceedings of the 19th IFAC Symposium on Automatic Control In Aerospace, Würzburg, 2013, p. 218–223.
[5] S. Busch, P. Bangert, F. Reichel, K. Schilling, The UWE satellite bus, a modular and flexible architecture for future picosatellite formations,

in: Proceedings of the 64th IAC Congress, IAC-13.B4.6B.3, Beijing, China, 2013.
[6] S. Busch, K. Schilling, UWE-3: a modular system design for the next generation of very small satellites, In: Proceedings of the Small Satellites Systems and Services – The 4S Symposium, Portoroz , 2012.
[7] N. Jones, Mini satellites prove their scientific power, Nature 508 (2014) 300–301.
[8] I. Kronhaus, M. Pietzka, K. Schilling, Pico-satellite formation control by electric propulsion, In: Proceedings of the 19th IFAC Symposium on Automatic Control in Aerospace, Würzburg, 2013.
[9] M. Swartwout, The first one hundred cubesats: a statistical look, J. Small Satell. 2 (2013) 213–233.
[10] F. Reichel, P. Bangert, S. Busch, K. Ravandoor, K. Schilling, The attitude determination and control system of the picosatellite UWE-3, In: Proceedings of the 19th IFAC Symposium on Automatic Control in Aerospace, Würzburg, 2013, p. 266–271.
[11] R. Sandau, S. Nakasuka, R. Kawashima, J. Sellers, Novel ideas for nanosatellite constellation missions, IAA Book Series, 2012.
[12] K. Schilling, F. Pranajaya, E. Gill, A. Tsourdos, Small satellite formations for distributed surveillance: system design and optimal control considerations, NATO RTO Lecture Series SCI-231, 2011.
[13] K. Schilling, M. Schmidt, S. Busch, Crucial technologies for distributed systems of pico-satellites, in: Proceedings of the 63rd International Astronautical Congress, IAC-12-D1.2.4, Naples, Italy 2012.
[14] S. Shirasaka S. Nakasuka, Concept of reasonably reliable systems engineering for micro-satellites, In: Proceedings of the 62nd International Astronautical Congress, IAC-11-B4.6A.8, 2011.